Received: 30 March 2020 | Revised: 21 August 2020 | Accepted: 14 September 2020

DOI: 10.1111/jace.17500



Journal of the American Ceramic Society

ORIGINAL ARTICLE

# Effect of moisture on the oxidation behavior of $ZrB_2$

**Ravisankar Naraparaju**[1] | **Keyur Maniya**[1] | **Alec Murchie**[2] | **William G. Fahrenholtz**[2] | **Gregory E. Hilmas**[2]

[1]German Aerospace Center (DLR), Institute of Materials Research, Cologne, Germany

[2]Department of Materials Science and Engineering, Missouri University of Science & Technology, Rolla, MO, USA

**Correspondence**
Ravisankar Naraparaju, German Aerospace Center (DLR), Institute of Materials Research, 51170, Cologne, Germany.
Email: ravisankar.naraparaju@dlr.de

**Abstract**

Oxidation studies of $ZrB_2$ were performed under wet air and dry air conditions at 1200°C, 1400°C, and 1500°C for 1, 4, and 10 h. Compared to dry air, the presence of water vapor was found to enhance the oxidation kinetics by a factor of 7 to 30, depending on the temperature. Thermodynamic calculations suggested that water vapor promoted the formation of additional volatile species such as boric acid ($HBO_2$), in addition to boria ($B_2O_3$) produced in dry air, which increased the evaporation rate of $B_2O_3$. Compared to dry air, the presence of water vapor leads to more rapid evaporation of boria and the transition from parabolic oxidation kinetic behavior (ie, rate controlled by diffusion through boria) to linear (ie, underlying $ZrB_2$ is directly exposed to the oxidizing environment) at shorter times and lower temperatures.

**KEYWORDS**

oxidation, ultra-high temperature ceramics, zirconia

## 1 | INTRODUCTION

Ultra-high-temperature ceramics (UHTCs) are a class of materials that include diborides (ie, $ZrB_2$, $HfB_2$), carbides (ie, ZrC, HfC), and nitrides (ie, ZrN, HfN) of early transition metals.[1] UHTCs have melting temperatures over 3000°C and the capability to tolerate extreme heating environments.[2-4] Increasing interest in hypersonic vehicles has led the development of new UHTC materials for wing leading edges and nose tips, as well as propulsion system components. Diboride-based UHTCs have performance advantages in some hypersonic applications compared to the carbides and nitrides due to better oxidation resistance and ability to transfer and redistribute heat (thermal conductivity > 100 W/m K at 25°C) at elevated temperatures.[5] Extensive research has been conducted over the years to understand the oxidation behavior of zirconium diboride ($ZrB_2$) in the low to high-temperature regimes. Previous studies have divided oxidation behavior into three regimes[6]: (a) the low-temperature regime below 1000°C where a crystalline zirconia ($ZrO_2$) and a continuous liquid/glassy boria ($B_2O_3$) scale form on the surface of the un-oxidized $ZrB_2$ matrix, providing passive oxidation protection. The oxidation kinetics in this regime is generally parabolic in nature. The oxidation rate is controlled by the diffusion of oxygen in the boria glass; (b) a second regime between 1000°C and 1800°C, where the evaporation of $B_2O_3$ begins in addition to the $ZrO_2$ formation and the final regime; and (c) a regime above 1800°C where the evaporation of $B_2O_3$ is rapid such that nearly all of the $B_2O_3$ is lost by evaporation and a porous $ZrO_2$ scale forms and offers no resistance to oxygen transport. Boria volatilizes over a wide range of conditions, such as various temperatures and partial pressures of oxygen in the external atmosphere, and $B_2O_3$ is the most predominant volatile species in air at 1500°C.[7] At temperatures above 1100°C in the presence of

water vapor, $HBO_2$(g) was the predominant gaseous species formed by oxidation of BN, although other species such as $H_3BO_3$ (g) and $H_3B_3O_6$ (g) become important at higher water vapor contents.[8] Historical studies on the oxidation behavior of pure $ZrB_2$ were mainly concentrated on understanding the effect of flow rate, oxygen partial pressure and external pressure.[9,10] In one of the studies, the rate of oxidation of $ZrB_2$ was found to be directly proportional to the oxygen partial pressure (100–740 Torr) within the temperature range of 945°C–1256°C.[11] In another study no oxygen pressure dependency at 1287°C and 1557°C was found.[10] Brown has observed an accelerated oxidation rate in pure oxygen compared to dry air and a much higher rate in moist air than in dry air in the temperature range 649°C–1315°C.[12] The effect of water vapor on the oxidation behavior of $ZrB_2$-SiC revealed that vapor enhances the oxidation rate by a factor of 2–3, which was attributed to the enhanced volatilization of silica.[13,14]

The purpose of this study was to analyze the effect of water vapor on the oxidation behavior of $ZrB_2$. Thermodynamic calculations and experimental studies of scale thickness as a function of temperature and time were combined to identify the underlying mechanisms.

## 2 | EXPERIMENTAL DETAILS

$ZrB_2$ specimens with relative densities of > 95% and average grain sizes of 19.3 ± 13.0 μm were used in the oxidation tests. Specimens were prepared by hot pressing commercial powders (Grade B, HC Starck) at 2100°C using 0.5 wt% carbon as a sintering aid. Details of the processing methods and microstructure analysis are described elsewhere.[15] Three types of oxidation experiments were performed in this study.

1. Oxidation under static ambient air (AA)
2. Oxidation under flowing synthetic air (SA)
3. Oxidation under flowing synthetic air + water vapor (SA + Bubbler)

Oxidation experiments were carried out in a box furnace (AA conditions, Netzsch) and a tube furnace consisting of a 1.5 m long alumina tube with an outer diameter of 10 cm (SA conditions, Nabertherm). The specimens were heated in alumina crucibles filled with zirconia powder to reduce the propensity for specimens to stick to the specimen support. Rectangular coupons were heated at 10°C/min to selected temperatures, which were 1200°C, 1400°C, and 1500°C, followed by isothermal holds of 1, 4, or 10 h under ambient air pressure (ie, nominally 1 atm). The coupons were cooled to room temperature at 10°C/min in the furnace. A flowmeter was used to control the flow rate of synthetic air (0.6 cm/s, linear flow rate was calculated from the volumetric flow rate and the diameter of the tube). For some SA experiments, a bubbler was used to saturate the SA with water prior to flowing into the furnace tube. The oxidized coupons were cut, mounted in a conductive epoxy, and polished using standard metallographic techniques to a 0.05 μm surface finish. Scanning electron microscopy (SEM) was performed using a DSM Ultra 55 (Carl Zeiss NTS, Wetzlar, Germany) microscope. SEM was equipped with an energy dispersive X-Ray spectroscopy (EDS) system (Inca, Oxford Instruments Abingdon, UK), which was used to determine compositions of oxide phases. The oxide scale thicknesses were measured and compared among all the specimens. Thicknesses were always measured at the center area of the coupon (ie, away from corners) and at least four to five measurements were made for each oxidation condition. X-ray diffraction (XRD) was used to identify the crystalline phases in the oxide scales. The XRD measurements were made using a Siemens D5000 diffractometer equipped with a CuKα radiation source with a secondary graphite monochromator (EVA/Topas 4.2 software package, Bruker AXS, Karlsruhe, Germany) directly on the oxidized specimens. Glow discharge optical emission spectroscopy (GDOES) is a technique based on identifying emissions from atoms by means from plasma by sputtering and GDA650 (Spectruma, Kleve, Germany) was used to identify boron oxide in the scale. Thermodynamic calculations were performed using the Equilib module of FactSage

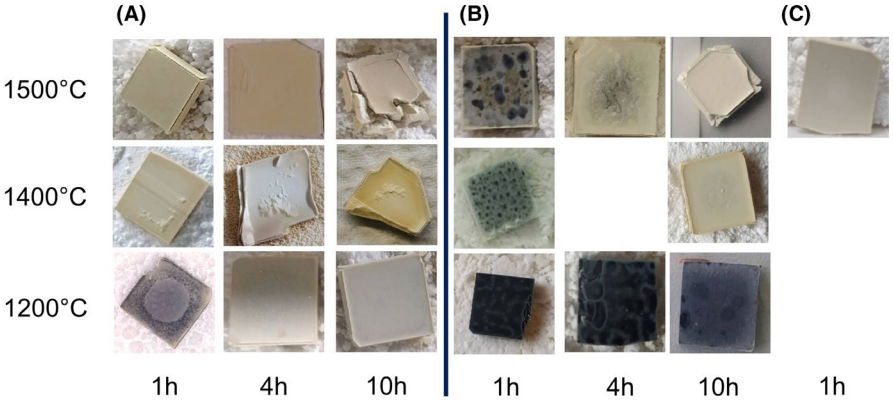


**FIGURE 1** Images of (A) $ZrB_2$ oxidized under AA and (B) $ZrB_2$ under SA conditions for different temperatures and times and (C) $ZrB_2$ under the SA + Bubbler condition. Nominal test specimen dimensions were 9 mm by 9-mm wide and 2.25-mm thick

7.3 using the FactPS database with the formation of all possible solid, liquid, and gas products. Calculations assumed that the activity of $B_2O_3$ (l) was unity and that the total pressure was maintained at 1 atm.

## 3 | RESULTS

### 3.1 | Oxidation experiments

Figure 1 shows the appearance of $ZrB_2$ coupons after oxidation. Figure 1A shows coupons oxidized under AA condition, whereas Figure 1B shows coupons oxidized under SA conditions. A clear difference in the oxide surfaces can be seen between the cases. Under SA, the surfaces were covered with a glassy layer (darker regions) for all oxidation times at 1200°C, in contrast to the brighter surfaces under AA (except for 1h which has moderate glassy surface) conditions. At 1400°C and 1500°C, specimens exhibited a glassy layer for the shorter oxidation periods under SA conditions. Nevertheless, only bright oxide was present at 1400 and 1500°C in case of AA condition.

Figure 2 shows the SEM micrographs of the oxide surface at 1200°C for 1h under SA and AA conditions. A few brighter grains were embedded in a glassy pool of boria (Figure 2A) in SA, whereas areas of dense bright crystals co-existed with boria glass for AA (Figure 2B). The hole encircled in the inset could be an evaporation route for boria or other gases produced during oxidation. Such holes were commonly found on the scale when examined at lower magnification (not shown). Boria is difficult to detect using EDS, and, as a result, GDOES was used on the darker regions of Figure 2A with the corresponding spectrum presented in Figure 2C. The peaks between 249 and 250 nm confirm the presence of boria based on previous reports. XRD was performed on the specimen oxidized for 4h at 1200°C under AA (Figure 2D). Monoclinic zirconia (m-$ZrO_2$) with lattice parameters of $a = 5.147$ Å, $b = 5.203$ Å and $c = 5.315$ Å was identified and indexed to JCPDS card 13-0307 from the ICDD database. This coupon had a uniform oxide scale with no glassy phase (ie, boria) on the surface, in contrast to the coupon oxidized at 1200°C for 1 h EDS analysis on brighter crystals of Figure 2B confirmed the presence of zirconia (See Figure 2E). From these measurements, the darker regions were identified as boria glass and the brighter oxide as m-$ZrO_2$.

### 3.2 | Oxidation kinetics

Oxide scale thicknesses from all the tested specimens are shown in Figure 3A. The oxide scale thickness increased with

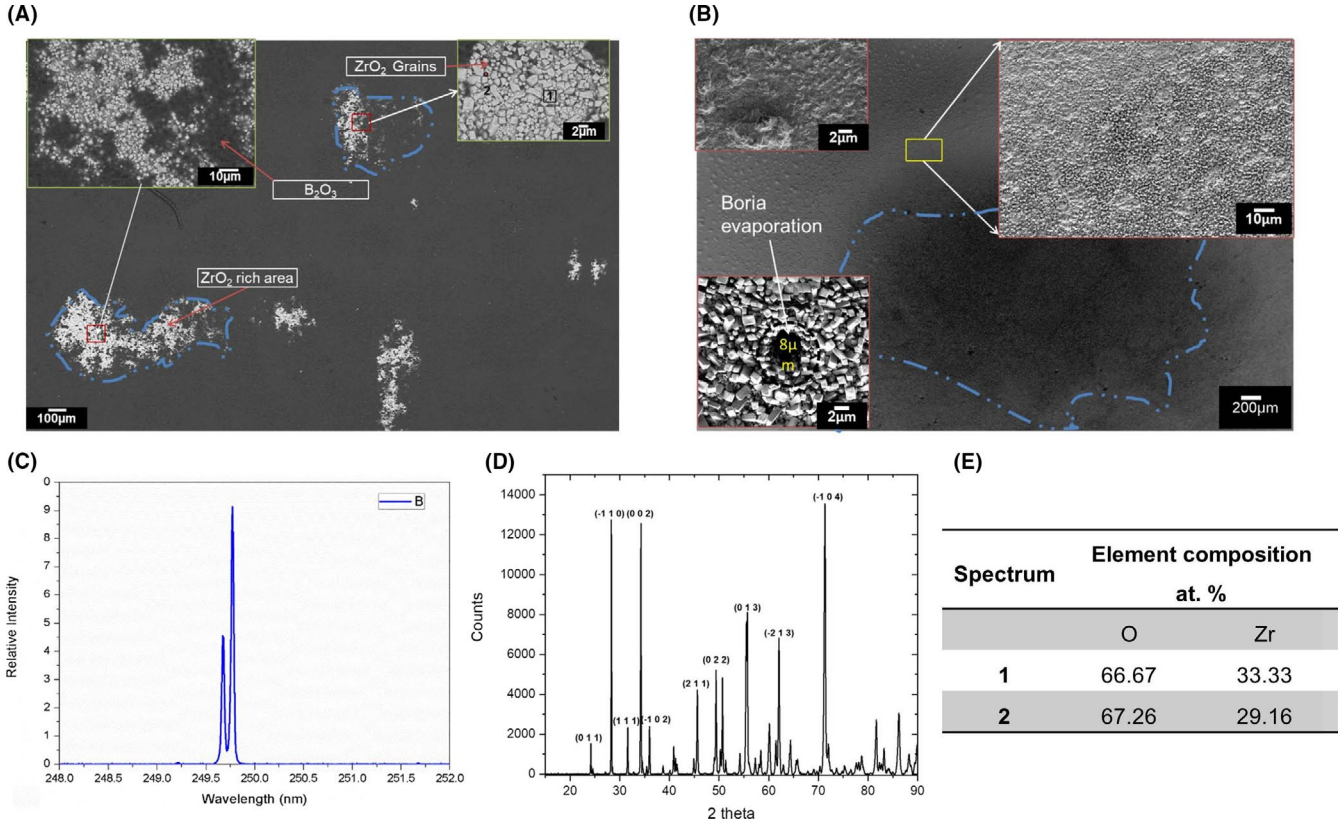


| Spectrum | Element composition at. % | |
|---|---|---|
| | O | Zr |
| 1 | 66.67 | 33.33 |
| 2 | 67.26 | 29.16 |

**FIGURE 2** SEM analysis of the surfaces of $ZrB_2$ coupons oxidized at 1200°C for 1 h under (A) SA, (B) AA conditions, (C) GDOES signal from the boria on (A), (D) XRD spectrum from the oxidized $ZrB_2$ for 4 h at 1200°C under AA condition and (E) EDS analysis of the white crystals shown on (B)

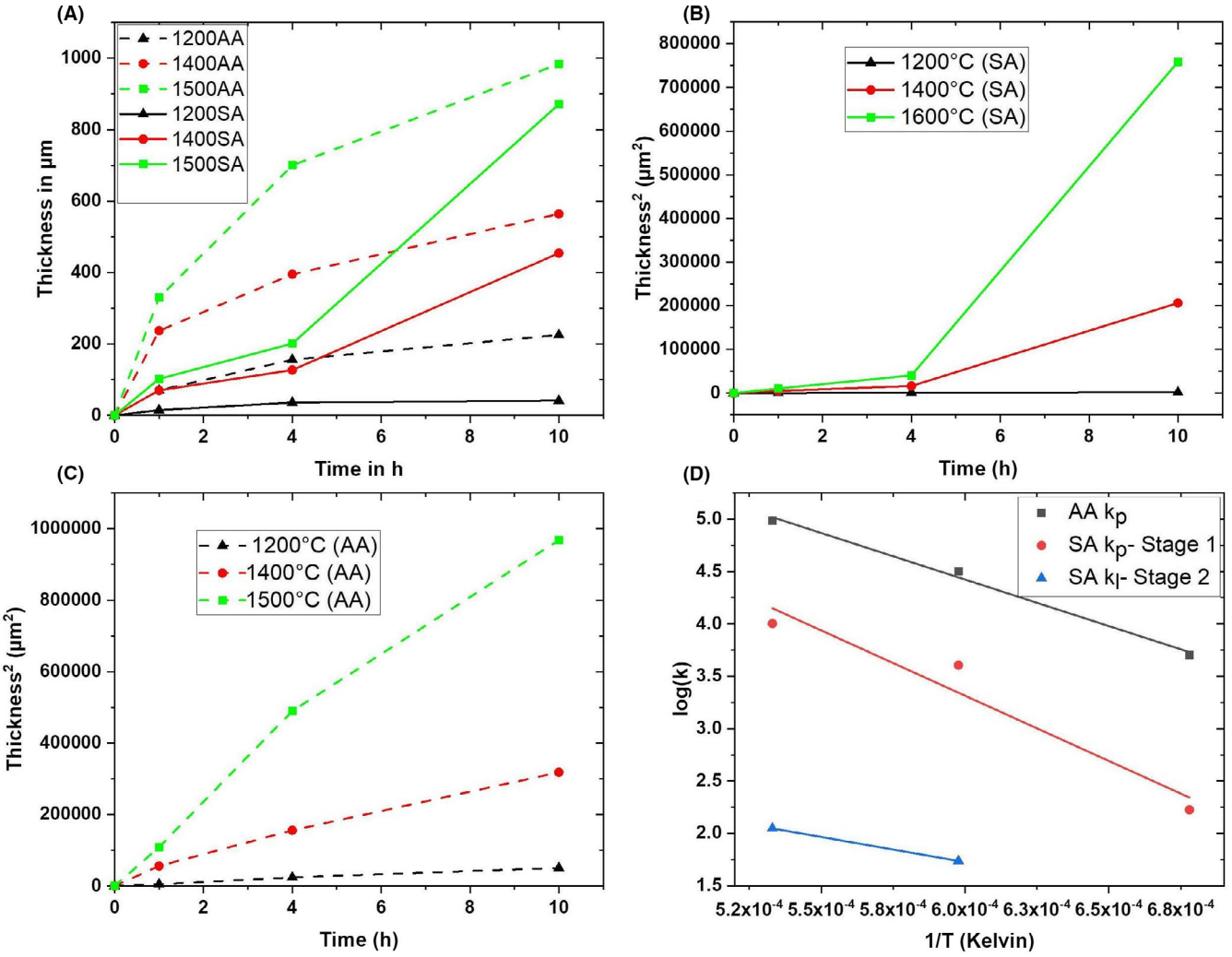


**FIGURE 3** (A) oxide scale thicknesses vs time for all the studied conditions, (B) (oxide scale thicknesses)$^2$ vs time for SA condition, (C) (oxide scale thickness)$^2$ vs time for AA condition and (D) log($k$) vs 1/$T$ for both AA and SA conditions showing the parabolic and linear growth of oxides of $ZrB_2$

**TABLE 1** Measured $ZrO_2$ oxide scale thicknesses of all the studied specimens

| Oxidation time (h) | Oxide scale thickness in µm | | | | | | |
|---|---|---|---|---|---|---|---|
| | 1200AA | 1400AA | 1500AA | 1200SA | 1400SA | 1500SA | 1500SA+Bubbler |
| 1 | 70 ± 10 | 237 ± 5 | 330 ± 50 | 15 ± 10 | 70 ± 40 | 102 ± 20 | 331 ± 9 |
| 4 | 156 ± 15 | 395 ± 15 | 700 ± 25 | 36 ± 20 | 127 ± 20 | 200 ± 20 | |
| 10 | 225 ± 5 | 564 ± 20 | 984 ± 25 | 41 ± 12 | 454 ± 25 | 871 ± 25 | |

respect to time at all temperatures. Separate plots of the square of thickness as a function of time are plotted in Figure 3B,C for SA and AA conditions. For SA condition, the oxidation rate seemed to follow a parabolic trend at 1200°C (straight line in the plot of thickness squared as a function of time), whereas at 1400 and 1500°C, the trend appeared to be transitioning to linear after 4h. In contrast, oxidation under AA resulted in a parabolic trend at 1200°C (straight line as shown in Figure 3C) as well as at 1400°C and 1500°C with increasingly positive curvature was observed with increasing temperatures. Nevertheless, thinner oxide scales were observed for SA compared to AA at all the temperatures. For example at 1200°C, zirconia scales were found to be 15 ± 10 µm thick after 1 h, 36 ± 20 µm thick after 4 h, and 41 ± 12 µm thick after 10 h for SA, whereas the scales were 70 ± 10 µm, 156 ± 15 µm, and 225 ± 5 µm thick for the same times for AA. For SA, at both 1400°C and 1500°C, the scale thickness increased more rapidly after 4 h under SA conditions (from 127 ± 20 µm to 454 ± 25 µm at 1400°C and from 200 ± 20 µm to 871 ± 25 µm at 1500°C). Because of the sudden increase in the thickness

between 4 and 10 h (Figure 3B), the oxidation behavior is divided into parabolic (stage 1) and linear (stage 2) regimes. All the measured oxide scale thicknesses for each condition are given in Table 1 and the corresponding rate constants have been calculated and are given in Table 2.

Activation energies have been calculated by plotting the log of rate constants as a function of reciprocal temperature. The activation energies were 73.4 kJ/mol for AA, 103.6 kJ/mol for SA stage 1, and 39.8 kJ/mol for SA stage 2.

## 3.3 | Oxide scale morphology

SEM cross-sectional images of the oxide scales grown after 4 h at 1200°C and 1400°C are presented in Figure 4, which show noticeable differences in the oxide scale morphology of the AA and SA conditions. The oxide scale for SA was considerably thinner than that of AA. For AA, the scale was 156 ± 10 μm thick after 4 h at 1200°C and 395 ± 15 μm after 4 h at 1400°C. In contrast for SA, the scales were 36 ± 20 μm and 127 ± 20 μm for SA conditions at the same temperatures and times. Moreover, the parallel "crack" type morphology was more apparent after oxidation in AA. Liquid boria may be present in these "crack" type pores, which would increase the resistance to oxygen diffusion. For oxidation in AA, the outer ~50 μm of the scale is free of these "crack" type pores after 4 h.

Figure 5A,B show the oxide scale morphology after oxidation for 4 h at 1500°C for AA and SA conditions. The oxide scale was ~500 μm thicker in the case of AA than SA. Moreover, the outer portion of the oxide scale (Figure 5A,B) contained larger pores, which might have formed due to the evaporation of boria and subsequent sintering of zirconia grains. The presence of parallel "crack" type pores was pronounced (about 80% of the scale) in the case of SA, whereas only the inner part of the scale produced in AA contained such features. The presence of columnar pores in the outer part of the scale produced in AA suggests the probable evaporation of boria. After 10 h, oxide scale morphologies were similar in both conditions (see Figure 5C,D) containing an outer porous layer and an inner relatively dense layer with "crack" type pores, although the oxide scale for AA was slightly thicker than for SA (984 ± 25 μm compared to 871 ± 25 μm). The outermost part of the oxide layer in SA was quite similar to that of AA 4 h exhibiting larger columnar poles.

**TABLE 2** Calculated oxidation rate constants for AA and SA conditions

| Condition | $k_p$ ($\mu m^2/h$) | $k_p$ ($\mu m^2/h$) (Stage1:1 to 4 h) | $k_l$ (μm/h) (Stage 2: 4 to 10 h) |
|---|---|---|---|
| 1200 AA | 5062 | | |
| 1400 AA | 31,809 | | |
| 1500 AA | 96,825 | | |
| 1200 SA | | 168 | — |
| 1400 SA | | 4032 | 55 |
| 1500 SA | | 10,099 | 112 |

The major difference between the two oxidation conditions other than using flowing air in SA condition was thought to be the presence of moisture for AA. To test this hypothesis, a new experiment was designed to add moisture to the flowing SA using a water bubbler. An additional oxidation test was carried out for 1h at 1500°C and the corresponding SEM cross-sectional micrograph of the oxide layer is presented in Figure 6C. The oxide scale thicknesses of the AA, SA, and SA + Bubbler after 1h at 1500°C are shown in Figure 6A–C, respectively. When water vapor was added to SA the oxide scale thickness (331 ± 9 μm, was shown as + in Figure 3A) matched that of ambient air (330 ± 50 μm). Moreover, the surface appearance of $ZrB_2$ coupons was also similar as shown in Figure 1A,C.

The oxide scale morphology was similar for both AA and the SA + Bubbler, but distinctly different from the morphology for SA. At 1400°C, the oxide scale produced in AA had two distinct porous zones (Figure 4C). The outer part of the scale consisted of equiaxed pores (see the inset in Figure 6B) surrounding a relatively denser inner zone with "crack" type pores nearer to the substrate. SA + Bubbler also produced similar zones where the oxide scale close to the substrate contained "crack" type pores. However, almost all the oxide scale produced in SA consisted of these parallel "crack" type pores (see Figure 6A). Boria glass was likely present in these pores before being removed by dissolution in water during metallographic preparation of the polished cross sections. The presence of boria in these pores would mean less evaporation of boria glass under these conditions and this implies thinner oxide scale compared to that of AA condition. An interesting trend in the "pore" structure with respect to oxidation time was observed for SA. After 1 h, the scale was predominantly "crack" type pores (after 1h). In contrast, after 4 h the scale was composed of two distinct layers with the outer part of the scale containing ~20% larger pores and the inner part and about 80% "crack" type pores in the inner part (see Figure 5B). After 10 h, the scale was very thick and it contained roughly equal portions of larger pores (outer part) and "crack" type of pores (inner part, see Figure 5D).

## 3.4 | Thermodynamic calculations

The volatility of boria under the conditions of the oxidation tests was assessed using thermodynamic calculations. The starting materials were one mole of $ZrB_2$ solid and 2.5 moles of oxygen gas along with the corresponding amount of nitrogen (9.4 moles assuming air was 21% oxygen and 79% nitrogen) that would be present in air. The water vapor pressure was assumed to be zero for dry air and 0.031 atm for wet air.

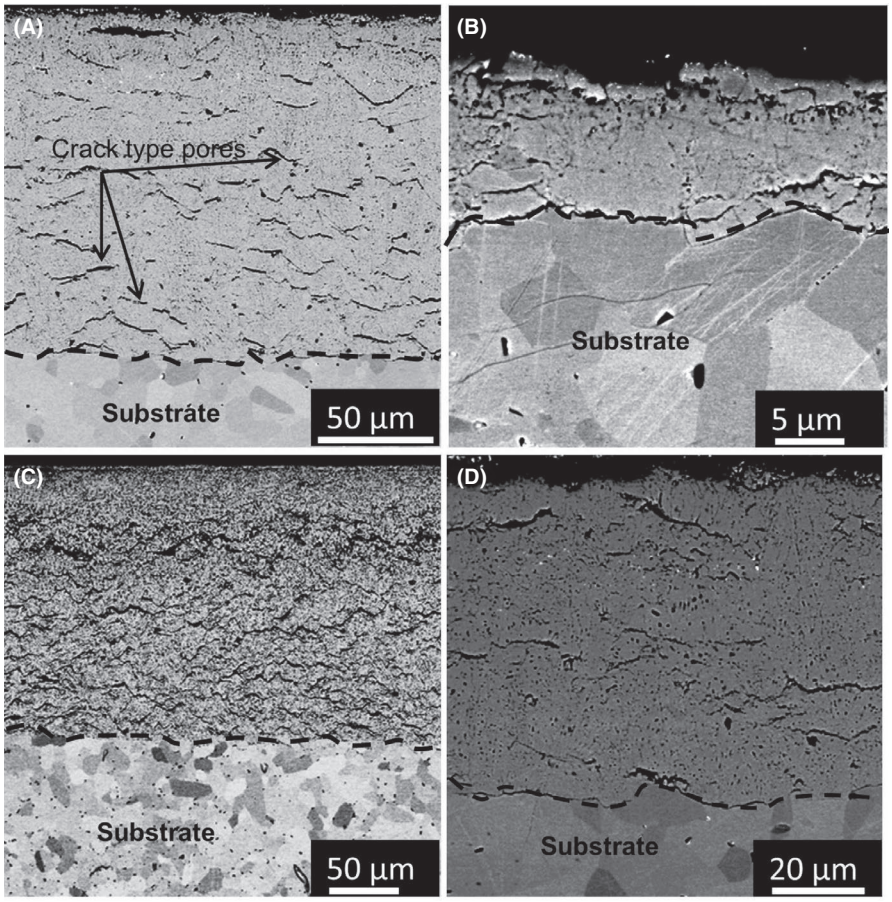


**FIGURE 4** Backscattered electron (BSE) images of cross sections of oxides grown on $ZrB_2$ after oxidation at (A) 1200°C AA, (B) 1200°C SA, (C) 1400°C AA, and (D) 1400°C SA after 4 h

This value was selected because it is the pressure for saturated water vapor pressure at 25°C,[16] as would be attained by bubbling air through water at room temperature prior to entering the furnace. For dry air, the predominant vapor species was $B_2O_3$ (g) at all temperatures. As expected the vapor pressure of $B_2O_3$ (g) increased with temperature from ~$10^{-5}$ atm at 1200°C to more than $10^{-3}$ atm at 1500°C. The presence of water vapor did not affect the predicted pressure of $B_2O_3$ (g), but the predominant species in the presence of water was $HBO_2$ with a vapor pressure that was 1 or 2 orders of magnitude higher than $B_2O_3$ at all temperatures (see Table 3).

Previous experimental studies have shown that boria evaporates readily during oxidation of $ZrB_2$ at 1500°C,[7] indicating that a vapor pressure on the order of $10^{-3}$ atm is sufficiently high to allow complete evaporation under conditions typically used for oxidation studies. The presence of water vapor promotes the formation of $HBO_2$ with a vapor pressure above $10^{-3}$ atm at 1200°C. Based on comparison to oxidation in dry air conditions, boria should volatilize more rapidly in the presence of water vapor due to the higher vapor pressure of $HBO_2$ under these conditions.

## 4 | DISCUSSION

The current results agree with previous reports that indicate that the oxidation of pure $ZrB_2$ follows parabolic kinetics at 1200°C under SA.[10,11] The kinetics become para-linear and linear in nature with increasing temperature.[4] The results show that the oxide formed at 1200°C was a mixture of boria (l) and zirconia (s). As temperature increased, boria evaporation left behind a porous zirconia scale.[5,6,10,11] As long as boria is present as a continuous layer, the reaction is controlled by diffusion through it, which we have observed in the 1200 SA condition. However, the continuous boria (l) outer scale was not present for AA condition (see Figure 1). The loss of the protective boria layer resulted in a loss of protection and thicker oxide scales compared to SA. With increasing temperature, oxidation kinetics were governed by the competition between the rates of boria formation and evaporation. The parallel "crack" type pores that were present at lower temperatures and shorter oxidation times were presumably filled with liquid boria, which offered protection against oxidation (Figure 4). In addition, AA has larger pores on the outer part of the coating suggests that probably higher boria evaporation than SA. At 1500°C, evaporation of boria was faster than its formation and the presence of larger pores in the outer part of the scale suggests that the oxidation rates have increased significantly. However, under SA, oxidation rates were lower up to 4h and the corresponding micrographs shown in Figure 6A and Figure 5B exhibit thinner oxide layers with mostly "crack" type pores. The porous outermost oxide

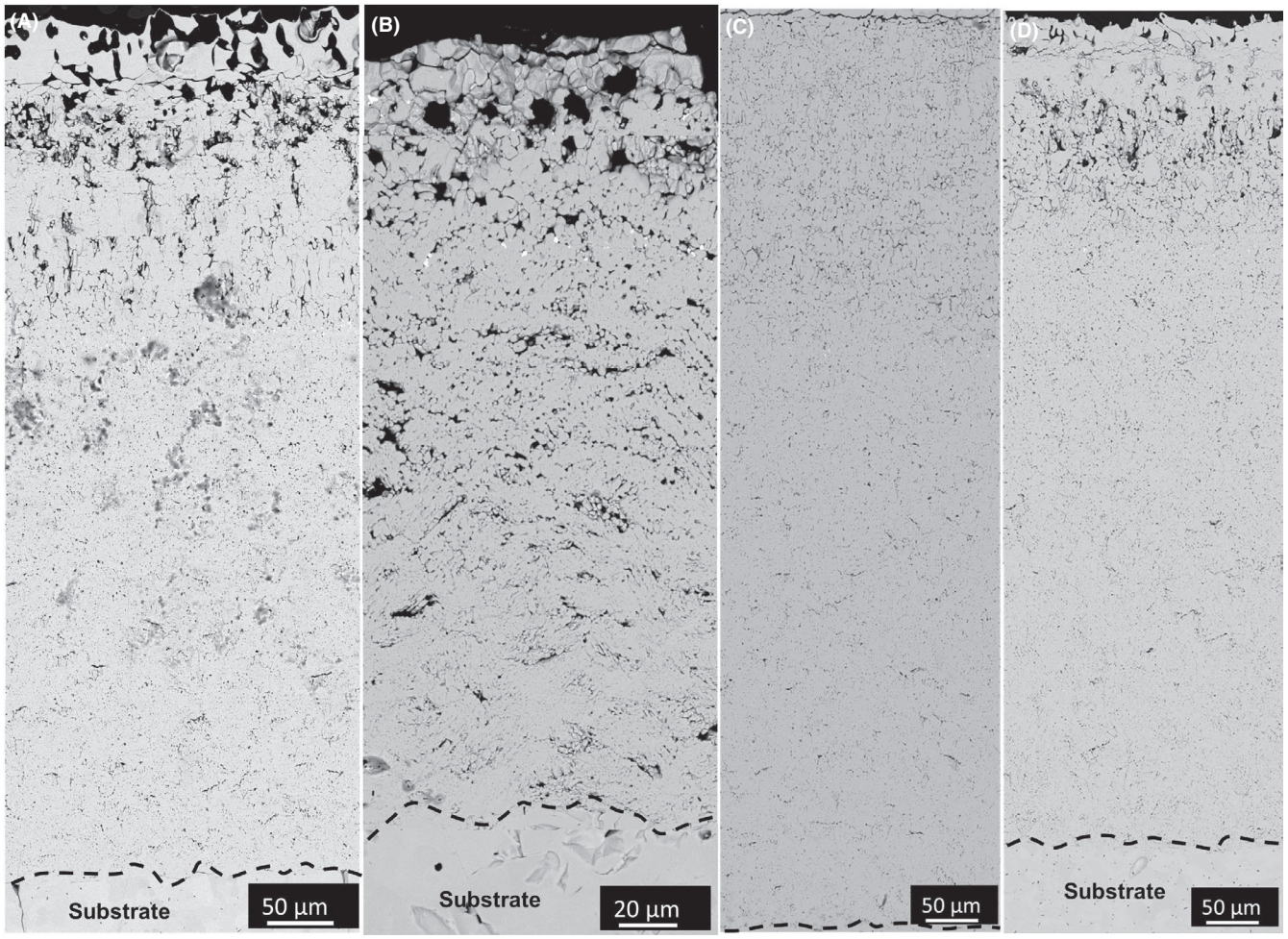


**FIGURE 5** BSE cross-sectional images of cross sections of oxides grown on $ZrB_2$ after oxidation at 1500°C for (A) AA, (B) SA after 4 h, (C) AA, and (D) SA after 10 h. Several micrographs are stitched together to show the complete oxide scale due to their larger thickness

layer after 4 h suggests the rapid evaporation of boria has started and a change in the oxidation rate can be expected. As shown in Figure 3B, the rate change occurred between 4-10 h. After 10 h under SA, the oxide scale was found to have similar pore morphology as in AA with comparable thickness. This implies that boria evaporation rate is also influenced by the oxidation time. The larger columnar pores in the upper part shown in Figure 5D are similar to that of 4h case under AA condition (Figure 5A: that is, faster evaporation of boria was delayed by a few hours under the presence of synthetic air. Zhang et al used similar experimental conditions (flowing synthetic air, at 1500°C with a heating/cooling rates of 5°C/min) and reported that a ~50-, 150-, and 500-µm-thick porous zirconia oxide scale had formed after 1, 2, and 3 h, respectively.[17] In another study, where slightly different oxidation conditions were used (flowing synthetic air at 1500°C, 5°C/min heating, and air quenching to room temperature) oxide scales of 30-, 60-, and 75-µm thick were reported after 1, 2 and 3 h.[18,19] Several factors influence oxidation scale thickness including air flow rate, cooling/heating rates, and measurement sensitivity in temperature. Kuriakose et al observed that the

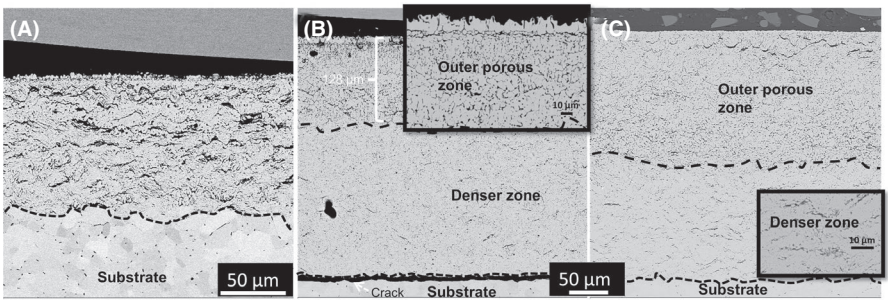


**FIGURE 6** BSE images of cross sections of oxides grown on $ZrB_2$ after oxidation at 1500°C for (A) SA, (B) AA and (C) SA + Bubbler after 1 h

**TABLE 3** Summary of predominant vapor species and vapor pressures for oxidation of $ZrB_2$ at different temperatures

| | Dry Air | | With water vapor | |
|---|---|---|---|---|
| | **Predominant species** | **Vapor pressure of predominant species (atm.)** | **Predominant species** | **Vapor pressure of predominant species (atm.)** |
| 1200°C | $B_2O_3$ | $1.3 \times 10^{-5}$ | $HBO_2$ | $3.5 \times 10^{-3}$ |
| 1400°C | $B_2O_3$ | $5.5 \times 10^{-4}$ | $HBO_2$<br>$B_2O_3$ | $1.6 \times 10^{-2}$<br>$5.5 \times 10^{-4}$ |
| 1500°C | $B_2O_3$ | $2.5 \times 10^{-3}$ | $HBO_2$<br>$B_2O_3$ | $2.7 \times 10^{-2}$<br>$2.5 \times 10^{-3}$ |

rate of oxidation of $ZrB_2$ was directly proportional to the oxygen partial pressure; however, no dependency of rate constants on flow rates was found at 1056°C.[11] The flow rate of synthetic air has a greater influence on the oxidation behavior at higher temperatures where the formation and evaporation of boria played greater roles in defining the oxidation kinetics. Our initial experiments showed a trend of decreasing oxidation rate with increasing flow rates of synthetic air at 1500°C, which is the subject of continuing study. In another study, the gas velocity was shown to be an important factor in volatility, spallation, and recession of UHTC materials.[13] Another important factor is the cooling and heating rates, which affect the length of time that specimens are exposed to oxidizing atmospheres. For example, a 5°C/min heating rate as used in Ref. [17] added an extra 60 mins of oxidation time in the temperature range from 1200°C to 1500°C to the overall oxidation time of 1, 2, and 3 h at 1500°C, compared to the higher heating rate used in the present study. The effect was different in another study,[18] using a 5°C/min heating rate and then quenching to room temperature at the end of the oxidation period. As a result, huge difference in the oxide scale thickness was observed (75 μm compared to 500 μm after 3 h at 1500°C) in both the studies.[17,18] To eliminate such effects, equal heating/cooling rates of 10°C/min were used in all the AA, SA, and SA + Bubbler conditions. As a result, measured oxide scale thicknesses in SA condition cannot be directly compared to other reported values without considering total oxidation time; however, our values were similar to those reported in the studies of Zhang et al.[17]

Significant differences were seen in the oxide scale thicknesses between AA and SA conditions at all the studied temperatures as shown in Figure 3. The difference in the oxide scale thicknesses can be explained by thermodynamic analysis of $ZrB_2$ oxidation. When $ZrB_2$ is exposed to dry air, the predominant vapor species is $B_2O_3$ (g), whereas other vapor species such as $BO_2$, $B_2O_2$, BO, $B_2O$, and $B_2$ have significantly lower vapor pressures.[7] The vapor pressure calculations presented in Table 3 predict a shift in the predominant vapor species and higher vapor pressures in the presence of water vapor, which should lead to increased evaporation of $B_2O_3$ at lower temperatures. At 1200°C, the vapor pressure of the predominant species in the presence of water vapor ($HBO_2$) was about the same as the vapor pressure of $B_2O_3$ in dry air at 1500°C. As a result of the increased vapor pressure, measurable boria evaporation starts at much lower temperatures when water vapor is present. The hole in the oxide scale shown in Figure 2B is evidence of such evaporation.

At 1400°C and 1500°C, the difference in the vapor pressures of predominant species is smaller, but still higher in air containing water vapor. At 1400°C, the vapor pressure of $HBO_2$ was about one order of magnitude higher than $B_2O_3$. The more rapid evaporation of the boria led to an increase in the thickness of the remaining zirconia scale. The abrupt increase in the oxide scale thickness between 4 and 10 h at 1400°C suggests a transition in oxidation mechanism at longer times. Presumably, the transition occurred when the boria no longer formed a continuous layer and the underlying $ZrB_2$ was directly exposed to the oxidizing environment.

At 1500°C in dry air, the vapor pressure of $B_2O_3$ is high enough to enable complete evaporation in flowing air. Since the air is flowing, it is not saturated in B-O species and continuous evaporation is promoted. The presence of water vapor still promoted the formation of $HBO_2$ which would enhance the evaporation rate compared to SA and could be responsible for the structural differences seen in Figure 1A. As a result of the presence of water vapor, higher oxidation rates with thicker zirconia scales form under static air conditions in the entire studied temperature range. The addition of water vapor to SA supports this hypothesis because SA containing water vapor would promote $HBO_2$ formation with a higher vapor pressure than boria vapor, which would lead to the increased thickness of the zirconia layer, similar to what was found for AA conditions.

## 5 | CONCLUSIONS

The following conclusions can be drawn from this study:

- The presence of water vapor increases the oxidation rate of $ZrB_2$ by promoting volatilization of the protective $B_2O_3$ at

lower and intermediate temperatures compared to dry air.

- The increased volatilization of boria, particularly at 1400°C and below, in the presence of water is due to the formation of a hydrated B-O compound, specifically $HBO_2$.
- This effect is severe at 1200°C, which causes oxidation to proceed with a linear oxidation rate in the presence of water vapor compared to parabolic kinetics in dry air.

## ACKNOWLEDGMENTS

At Missouri University of Science and Technology, this research was supported by the Enabling Materials for Extreme Environments signature areas. Alec Murchie was supported by a Graduate Assistance in Areas of National Need (GAANN) fellowship. The authors acknowledge Andrea Ebach-Stahl (DLR) for her assistance in conducting GDOES measurements. The authors acknowledge Dr Mechnich for his assistance in water vapor experiments using bubbler. Open access funding enabled and organized by Projekt DEAL

## ORCID

*Ravisankar Naraparaju* https://orcid.org/0000-0002-3944-1132
*Gregory E. Hilmas* https://orcid.org/0000-0002-8497-0092

## REFERENCES

1. Wuchina E, Opila E, Opeka M, Fahrenholtz W, Talmy I. UHTCs: ultra-high temperature ceramic materials for extreme environment applications. Electrochem Soc Interface. 2007;16(4):30–6.
2. Silvestroni L, Kleebe HJ, Fahrenholtz WG, Watts J. Super-strong materials for temperatures exceeding 2000°C. Sci Rep. 2017;7:40730.
3. Opeka MM, Talmy IG, Wuchina EJ, Zaykoski JA, Causey SJ. Mechanical, thermal, and oxidation properties of refractory hafnium and zirconium compounds. J Eur Ceram Soc. 1999;19(13–14):2405–14.
4. Fahrenholtz WG, Wuchina EJ, Lee WE, Zhou Y, editor. Ultra high temperature ceramics: materials for extreme environment applications. Hoboken, NJ: JOHN WILEY & Sons, Inc.; 2014.
5. Fahrenholtz WG, Hilmas GE. Oxidation of ultra-high temperature transition metal diboride ceramics. Int Mater Rev. 2013;57(1):61–72.
6. Parthasarathy TA, Rapp RA, Opeka M, Kerans RJ. A model for the oxidation of $ZrB_2$, $HfB_2$ and $TiB_2$. Acta Mater. 2007;55(17):5999–6010.
7. Fahrenholtz WG. The ZrB2 volatility diagram. J Am Ceram Soc. 2005;88(12):3509–12.
8. Jacobson N, Farmer S, Moore A, Sayir H. High-temperature oxidation of boron nitride: I, monolithic boron nitride. J Am Ceram Soc. 1999;82(2):393–8.
9. Kaufman L, Clougherty EV, Berkowitz-Mattuck BB. Oxidation characteristics of Hafnium and zirconium diboride. Trans Metall Soc AIME. 1967;239:458–66.
10. Tripp WC, Graham HC. Thermogravimetric study of the $ZrB_2$ in the temperature range of 800°C to 1500°C. Solid State Sci. 1971;118:1195–9.
11. Kuriakose AK, Magrave JL. The oxidation kinetics of zirconium diboride at high temperature. J Electrochem Soc. 1964;111:827–31.
12. Brown FHJ. Progress Report No. 20–252. Pasadena, CA: Jet Propulsion Laboratory; 1955.
13. Nguyen QN, Opila EJ, Robinson RC. Oxidation of ultrahigh temperature ceramics in water vapor. NASA/TM-2004-212923; 2014.
14. Guérineau V, Julian-Jankowiak A. Oxidation mechanisms under water vapour conditions of ZrB2-SiC and HfB2-SiC based materials up to 2400°C. J Eur Ceram Soc. 2018;38(2):421–32.
15. Neuman EW, Hilmas GE, Fahrenholtz WG. Processing, microstructure, and mechanical properties of large-grained zirconium diboride ceramics. Mater Sci Eng A. 2016;670:196–204.
16. Rumble JK, editor. Handbook of chemistry and physics, 62nd edn. CRC: Boca Raton, FL; 1981.
17. Zhang SC, Hilmas GE, Fahrenholtz WG. Improved oxidation resistance of zirconium diboride by tungsten carbide additions. J Am Ceram Soc. 2008;91(11):3530–5.
18. Kazemzadeh Dehdashti M, Fahrenholtz WG, Hilmas GE. Oxidation of zirconium diboride with niobium additions. J Eur Ceram Soc. 2013;33(10):1591–8.
19. Kazemzadeh Dehdashti M, Fahrenholtz WG, Hilmas GE. Effects of transition metals on the oxidation behavior of ZrB2 ceramics. Corros Sci. 2015;91:224–31.

**How to cite this article:** Naraparaju R, Maniya K, Murchie A, Fahrenholtz WG, Hilmas GE. Effect of moisture on the oxidation behavior of $ZrB_2$. *J Am Ceram Soc.* 2020;00:1–9. https://doi.org/10.1111/jace.17500